Nano Energy 133 (2025) 110491

Contents lists available at ScienceDirect

Nano Energy

journal homepage: www.elsevier.com/locate/nanoen

Innovative smart gloves with Phalanges-based triboelectric sensors as a dexterous teaching interface for Embodied Artificial Intelligence[☆]

Long Liu [a,b,*,1], Tong Hu [a,b,1], Xinmao Zhao [a,b,1], Yifeng Su [a,b], Dezhi Yin [a,b], Chengkuo Lee [c,d,**], Zhong Lin Wang [e,f,***]

[a] School of Electronics and Information, Northwestern Polytechnical University, Xi'an 710072, China
[b] Research & Development Institute of Northwestern Polytechnical University in Shenzhen, Shenzhen 518063, China
[c] Department of Electrical and Computer Engineering, National University of Singapore, Singapore 117583, Singapore
[d] Center for Intelligent Sensors and MEMS (CISM), National University of Singapore, Singapore 117608, Singapore
[e] Beijing Institute of Nanoenergy and Nanosystems, Chinese Academy of Sciences, Beijing 101400, China
[f] School of Material Science and Engineering, Georgia Institute of Technology, Atlanta, GA 30332, USA

ARTICLE INFO

Keywords:
Triboelectric nanogenerator
Self-powered sensor
Teaching interface
Human-machine interface
Embodied artificial intelligence

ABSTRACT

Embodied Artificial Intelligence (EAI) enables robots to autonomously learn through complex interactions with the external world, enhanced by integrated speech and vision capabilities for effective communication with users. In contrast, human learning initially occurs without speech, where gestures function as a potent educational instrument and a vital communication mode. This work presents a type of smart glove that utilizes triboelectric nanogenerators (TENGs) and is specifically engineered to function as an advanced teaching interface for EAI (Ti-EAI) in facilitating interactions between humans and robots. The Phalanges-based Triboelectric Sensor (PTS) boasts a segmented design that conforms to finger movements, thereby minimizing sensor interference and guaranteeing natural motion. A linkage mechanism featuring a double-layer electrode design with a phase difference has been integrated to optimize signal outputs and enrich the gesture information embedded within the signals. Within the Ti-EAI system, the human operator utilizes PTS-enabled gloves as an instructional medium to systematically impart directives and knowledge to the robots. This configuration significantly enhances the robot's ability to perceive environmental subtleties by leveraging gesture-based communication, improving its intrinsic intelligence. The Ti-EAI system enables robots to autonomously recognize gestures, engage in logical interactions through subjective actions, and sustain a continuous dialogue through the utilization of a large-scale model. Notably, the findings from this system illustrate substantial progress in EAI, thereby broadening its application scope within humanoid robots and facilitating a deeper integration into diverse daily life contexts.

1. Introduction

Embodied Artificial Intelligence (EAI), a crucial subfield of artificial intelligence, endeavors to attain brain-like capabilities via active perception utilizing multiple sensors, long-term simulation facilitated by integrated algorithms, and continuous improvement throughout interactions[1–3]. This approach implies that autonomous learning can progressively enhance sensory and cognitive abilities[4,5]. For robots, the physical manifestations of embodied artificial intelligence (EAI), developing perception, comprehension, and interaction capabilities necessitates external assistance, primarily facilitated through acquiring sensory information and applying machine learning techniques[6–9].

☆ "Prof Zhong Lin Wang, an author on this paper, is the Editor-in-Chief of Nano Energy, but he had no involvement in the peer review process used to assess this work submitted to Nano Energy. This paper was assessed, and the corresponding peer review managed by Professor Chenguo Hu, also an Associate Editor in Nano Energy"

* Corresponding author at: School of Electronics and Information, Northwestern Polytechnical University, Xi'an 710072, China.
** Corresponding author at: Department of Electrical and Computer Engineering, National University of Singapore, Singapore 117583, Singapore.
*** Corresponding author at: Beijing Institute of Nanoenergy and Nanosystems, Chinese Academy of Sciences, Beijing 101400, China.
E-mail addresses: longerliu@nwpu.edu.cn (L. Liu), elelc@nus.edu.sg (C. Lee), zlwang@gatech.edu (Z.L. Wang).

[1] These authors contributed equally.

https://doi.org/10.1016/j.nanoen.2024.110491
Received 29 September 2024; Received in revised form 11 November 2024; Accepted 18 November 2024
Available online 22 November 2024
2211-2855/

Despite significant advancements over the years, the intelligence exhibited by current EAI systems remains markedly inferior to human levels, underscoring the imperative for further research to comprehensively understand human cognition and develop systems capable of emulating these intricate cognitive processes[10,11]. Human cognitive development is a multifaceted and protracted process that inherently encompasses auditory perception and stimulation, the acquisition of linguistic competence, visual discrimination, and observation, as well as the imitation of actions and behaviors[12,13]. Humans, initially devoid of innate linguistic abilities, primarily engage with their surroundings through gestures and prelinguistic vocalizations from teaching, progressively acquiring sophisticated communication abilities over time via exposure to linguistic inputs and social interactions[14]. Constructing a Teaching interface for EAI (Ti-EAI) with advanced sensing technologies is therefore essential for assessing and enhancing robot intelligence, as it enables robots to achieve a deeper understanding of complex concepts and tasks while allowing users to act as educators[15,16].

To seamlessly augment the robot's cognitive capabilities within the TI-EAI, data gloves can be employed to precisely capture the educator's hand movements. The integration of advanced sensors, such as bending sensors[17–20], inertial measurement units (IMUs)[21,22], and force sensors[23], significantly enhances human-robot interaction. However, traditional sensors face limitations, particularly in scenarios requiring prolonged operation, due to their reliance on external power sources. To overcome these challenges, novel self-powered sensors are being developed, with triboelectric sensors offering diverse material options and flexible structural designs[24–33]. In recent years, numerous research articles have reported advancements in triboelectric nanogenerators (TENGs) for smart gloves, thereby expanding their application range. For instance, Fang et al. introduced a starch-based hydrogel sensor with multimodal sensing capabilities[34]. By utilizing strain-sensing gloves to capture finger flexion signals, remote human-machine operation can be achieved. Xiong et al. integrated flexible sensors into textile gloves, designing a recognition system that serves as an interactive interface and can perform rescue tasks in hazardous situations when combined with lidar[35]. Additionally, Zhang et al. utilized 3D-printed smart sensing gloves for gaming, enabling gesture-based control for smart home systems[36]. However, with the emergence and development of EAI, human understanding of intelligence levels continues to evolve. These sensing gloves often lack the capability to interpret genuine human intentions and fail to accurately map complex hand movements[37–40]. Therefore, designing triboelectric sensors that accommodate joint and inter-joint activities can effectively convey authentic information, aiding in the decoupling of intricate dynamic gestures. Furthermore, many researchers have employed artificial intelligence (AI) methods to deepen the understanding of sensing mechanisms[41–44]. The integration of flexible triboelectric sensors with machine learning algorithms, particularly neural networks, facilitates effective real-time data analysis, thereby further refining the development of embodied agents[45,46].

To enhance human-machine interaction capabilities and empower embodied agents to elevate their intelligence through imitation of human behavior, this paper introduces an innovative Phalanges-based Triboelectric Sensor (PTS), which is meticulously designed to conform precisely to the three-stage joint flexion structure of the human finger and incorporates triboelectric nanogenerators (TENGs) to construct self-powered sensing channels. By digitizing the flexion states, the PTS employs a multi-channel differential electrode design to accurately capture various bending angles and flexion/extension states of finger joints, thereby facilitating advanced artificial intelligence analysis with human teacher gesture inputs. This theoretical framework enables the differentiation of multiple joints within a single finger and the recognition of similar gesture movements via smart gloves equipped with PTSs. The signal amplification, influenced by variations in phase, amplitude, and peak counts between upper and lower circuits, generates multidimensional signals that support dynamic and static interactions, allowing for precise action prediction when integrated with deep learning algorithms. Furthermore, the integration of large-scale model technologies and Unity3D vision-design capabilities enables the transmission of the operator's cognitive intentions to the robotic system, thereby achieving a form of "remote brain-to-robot connectivity." Together with gesture and voice recognition technologies, this system progressively acquires capabilities for communication, logical reasoning, and interactive gaming, evolving into a comprehensive intelligent entity.

2. Results and discussion

2.1. Concept and design of a robotics teaching platform

As exemplified in Fig. 1, this research presents an intelligent glove designed to serve as an interface for Embodied Artificial Intelligence (Ti-EAI). Specifically, Fig. 1a portrays a scenario in which a human donning the intelligent glove functions as an instructor for a robot, creating an autonomous teaching interface that facilitates the robot's accurate imitation of human actions. The primary objective of TAI is to augment the robot's embodied intelligence, empowering it to independently execute tasks encompassing gesture recognition, interactive actions, and sustained dialogue.

The glove is equipped with the Phalanges-based Triboelectric Sensor (PTS), which employs a freestanding triboelectric nanogenerator to produce electrical signals through friction between materials with differing electronegativities (Fig. 1b). To ensure unimpeded hand movement, as illustrated in Fig. 1c and S1, the PTS is engineered to conform to the three-segment bending structure of the fingers and is mounted on the glove's outer surface, facilitating rapid attachment and detachment. The information outlined in Table S1 reveals that our proposed PTS achieves broad functionality with a simplified design and common materials, marking a substantial advancement when juxtaposed with prior works. By incorporating an innovative dual-layer electrode design, the sensor transcends mere directional signal acquisition, integrating novel data pathways that enrich the dataset for deep learning-based gesture recognition. Similarly, through integration with large language models, our smart glove surpasses the limitations of basic gesture recognition, enabling complex logical interactions, real-time adaptability, and voice communication capabilities, thereby establishing a new benchmark for gesture recognition performance. Furthermore, the integration of Bluetooth Low Energy (BLE) technology facilitates efficient and reliable remote wireless data transmission. Presented in Figure S2, our design encapsulates a wide array of advanced benefits, making it highly versatile for real-time applications.

2.2. Design, preparation, and principles of the PTS

The design details of the PTS are illustrated in Fig. 2a, and the different colors in Fig. 2a(i) indicate the required friction materials. As depicted in Fig. 2a(ii), for the mobile end, EVA foam tape is double-sided and adhered to a PVC film, which is then laser-cut into small components matching the joint length to form a supportive framework. Copper foil electrodes of varying widths are attached above and below this framework (Figure S3). In addition, the lightweight construction (only 3.28 g) allows for closer contact between the glove and the fingers, reducing unnecessary friction and pressure, thus avoiding the discomfort that may be associated with prolonged wear (Figure S4). For the fixed end of the pipeline, an FEP film covers the interdigital electrodes as a critical friction material. As shown in Fig. 2a(iii), utilizing the segmented design of the finger joints drives the linkage structure to slide within the pipeline of the fixed end. Except for the thumb, the entire mobile end is 1.5 centimeters wide (slightly wider than the finger) to prevent interference between adjacent fingers. The fixed end of the pipeline is based on a width of 1.5 cm, with a slightly wider pipeline formed by a PET ring structure employing an arched design. The longer

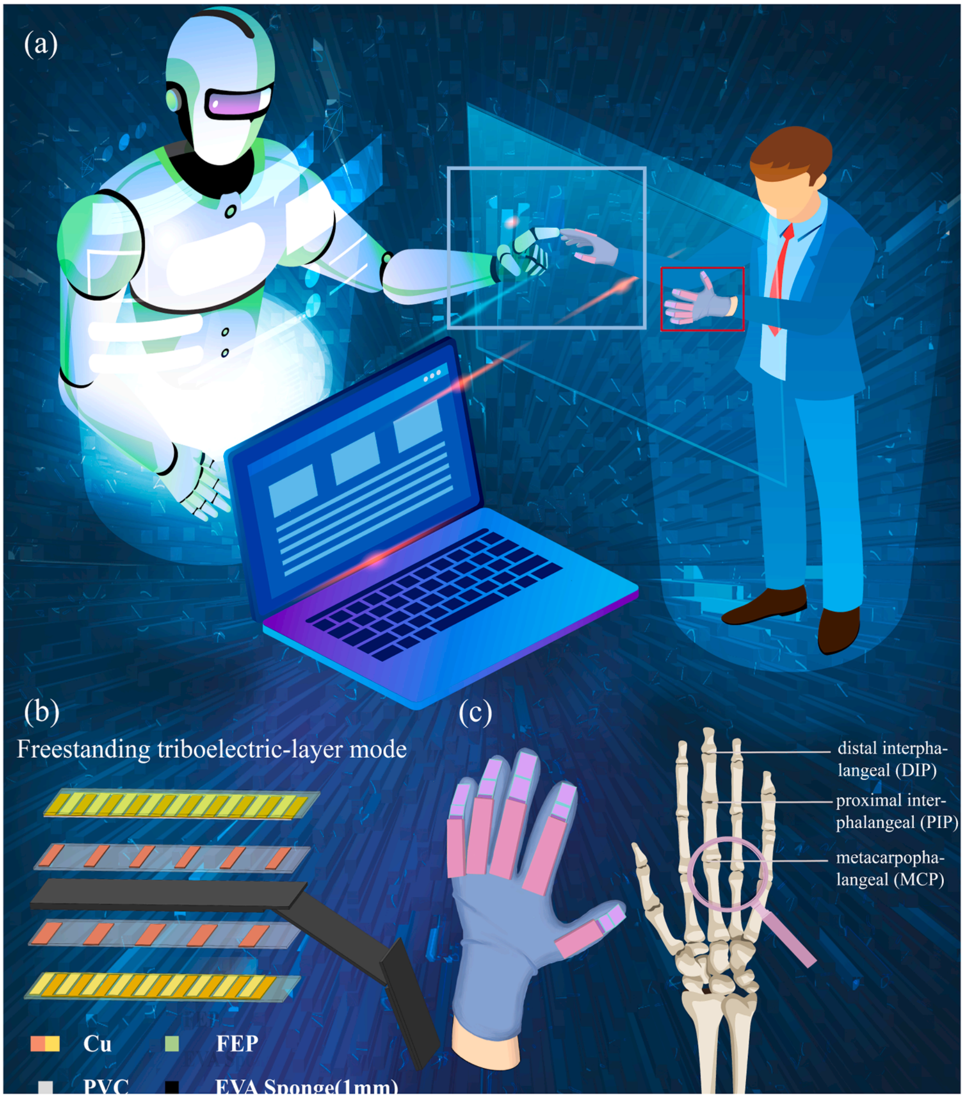

Fig. 1. Robotic Intelligent Education System Based on Intelligent Sensing Gloves. (a) By wearing smart data gloves, it is possible to construct an educational interface to realize the robot's imitation of human movements. (b) Detailed view of a freestanding triboelectric-layer mode sensor based on the difference in electronegativity of the friction material that generates signal output. (c) Rendering of a hand wearing a smart glove. The sensor is designed to satisfy the three joint bending structure of the fingers.

FEP bends inward at the junctions between adjacent electrodes, thereby increasing the contact area with the mobile end and preventing signal discharge. The design facilitates smooth sliding of the mobile end within the confines of the fixed end, ensuring a seamless and efficient operational mechanism.

Fig. 2b(i) displays the schematic that has been produced, depicting a transparent PVC strip linked to the glove's exterior at the fingertip. The primary section is partitioned into three segments, as seen in Fig. 2b(ii): 1) The mobile end is the part that moves along with the joint. 2) The horizontal end is the part that glides into contact with the interdigital electrodes. 3) The fixed end is the part of the pipeline that remains stationary at the joint. The different lengths of the movable end enable the attachment to bend as the joint moves downward and prevent any blockage when the finger extends. The intrinsic interaction between the finger joint and the segmented construction causes the final segment to slip within the finger-attached pipeline. The position of the final segment within the fixed pipeline may be determined by employing the TENG method. The beginning point for interdigital electrode insertion in the pipeline is the leftmost end, located near the palm. It eliminates any contact irregularities the segmented joint construction may produce.

An intuitive understanding of the output mechanism of the TENG is provided through the overlapping electron cloud (OEC) model. As depicted in Fig. 2c, varying interaction potentials occur between two contacting objects depending on whether they are at the equilibrium position, in the repulsive zone, or in the attractive zone. Fig. 2d illustrates two scenarios: initially, before atomic-scale contact between the two materials (in the attractive zone), their respective electron clouds remain separate without any overlap. As the contact area increases, the electron clouds begin to overlap (in the repulsive zone), transforming the initial single potential well into an asymmetric double potential well, enabling the transfer of electrons between the two atoms. On the basis of this, the finger flexion state sensing functions by utilizing the operational principle of a freestanding triboelectric-layer mode TENG. Charge transfer transpires across the external circuit as a result of disparities in the contact area within the system. Fig. 2e shows the segmentation of the electrodes into A-Phase and B-Phase. The difference in electronegativity between copper and FEP causes the formation of positive charges on the surface of copper, resulting in the achievement of equilibrium in stage (i). Upon the lateral displacement of the triboelectric layer towards the right (spanning from stage i to iv), positive charges migrate in a leftward direction, inducing a temporary flow of current within the external circuitry. Attributable to the expanded contact interface inherent to the

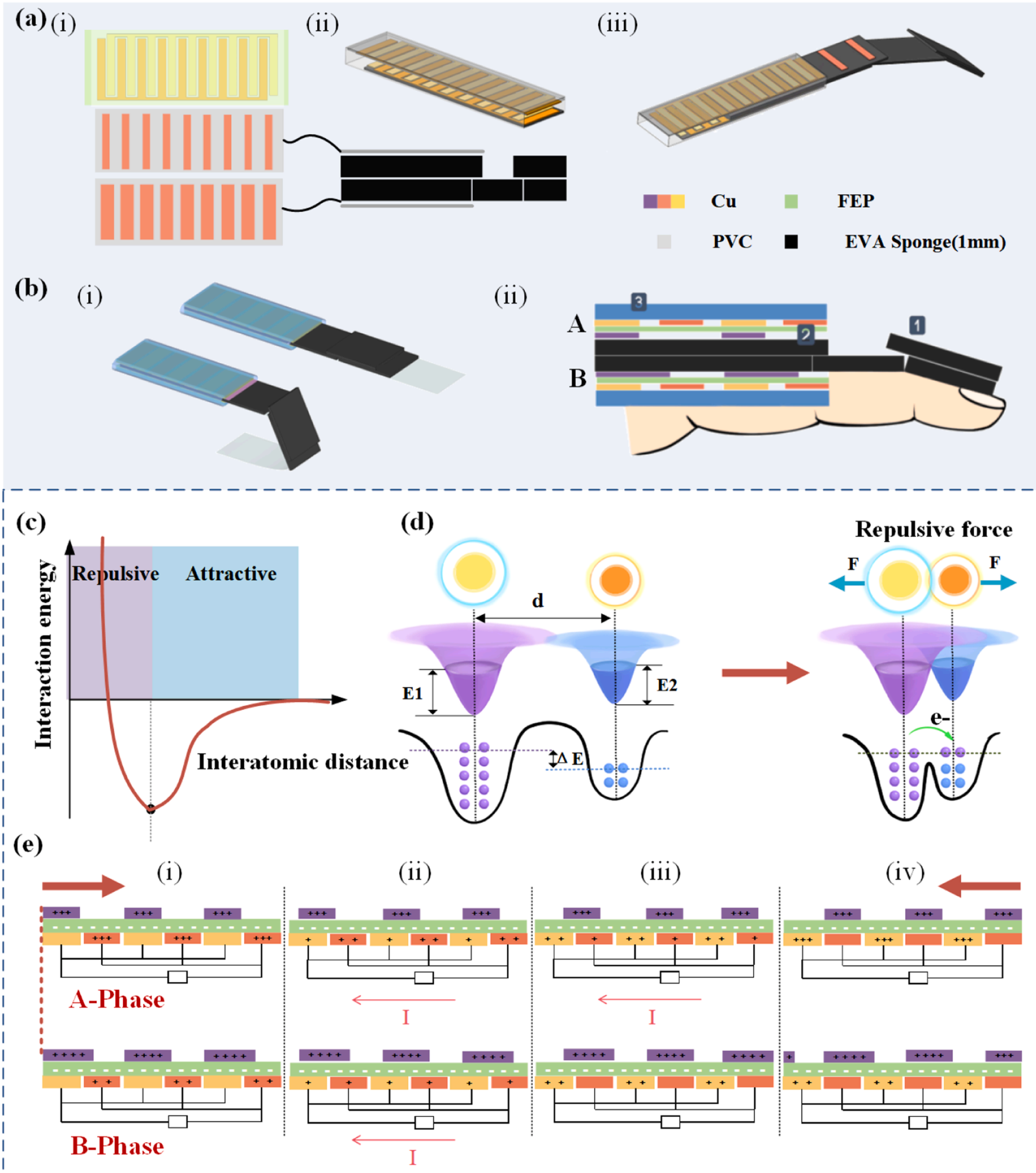

Fig. 2. The construction and operational principles of the sensor. (a) Depicts the fabrication process of the wearable sensor peripheral equipment for capturing hand movement gestures. (b)A rendering and its structural schematic: 1) Mobile end; 2) Horizontal end; 3) Fixed pipe end. (c)The interaction energy of two atoms in different regions. (d)The overlapped electron-cloud model. (e)Elucidates the working principle of the multi-channel design sensor based on freestanding triboelectric-layer mode TENG.

B-Phase, the process of charge transfer is expedited, achieving a novel charge equilibrium as early as stage iii. In stark contrast, the A-Phase achieves full charge transfer only upon perfect alignment, demonstrating an elongated charge transfer period. Conversely, during the reverse sliding motion from stage iv back to i, there is an absence of charge transfer between stages iv and iii, leading to a delayed initiation of the B-Phase in comparison to the A-Phase. Nevertheless, upon the concurrent alignment of the left termini of both components, the voltage returns to a zero potential simultaneously, generating a phase disparity that originates from their differing commencement times. This meticulously engineered phase difference significantly enhances the recognition capabilities of our apparatus, establishing a robust foundation for highly efficient gesture recognition and real-time interactive capabilities.

2.3. Differential amplification circuit and dual channel phase difference principle

Triboelectric signals are commonly defined by their small magnitude and vulnerability to external disturbances and electromagnetic interference. Simultaneously, it is crucial to have a design that includes high input impedance, broad bandwidth, and low power consumption to guarantee precise amplification and steady transmission of the signal. To enhance the signal's resistance to interference and efficiently reduce common-mode noise, a dual operational amplifier (LM358P) is used for the differential design. Fig. 3a displays the circuit diagram of the signal processing circuit. The power supply module comprises a portable battery box and three series-connected 1.5-volt batteries. To meet the single-supply requirement, a DC bias is added to the generated sinusoidal AC signal to achieve the positive half-axis voltage. A voltage

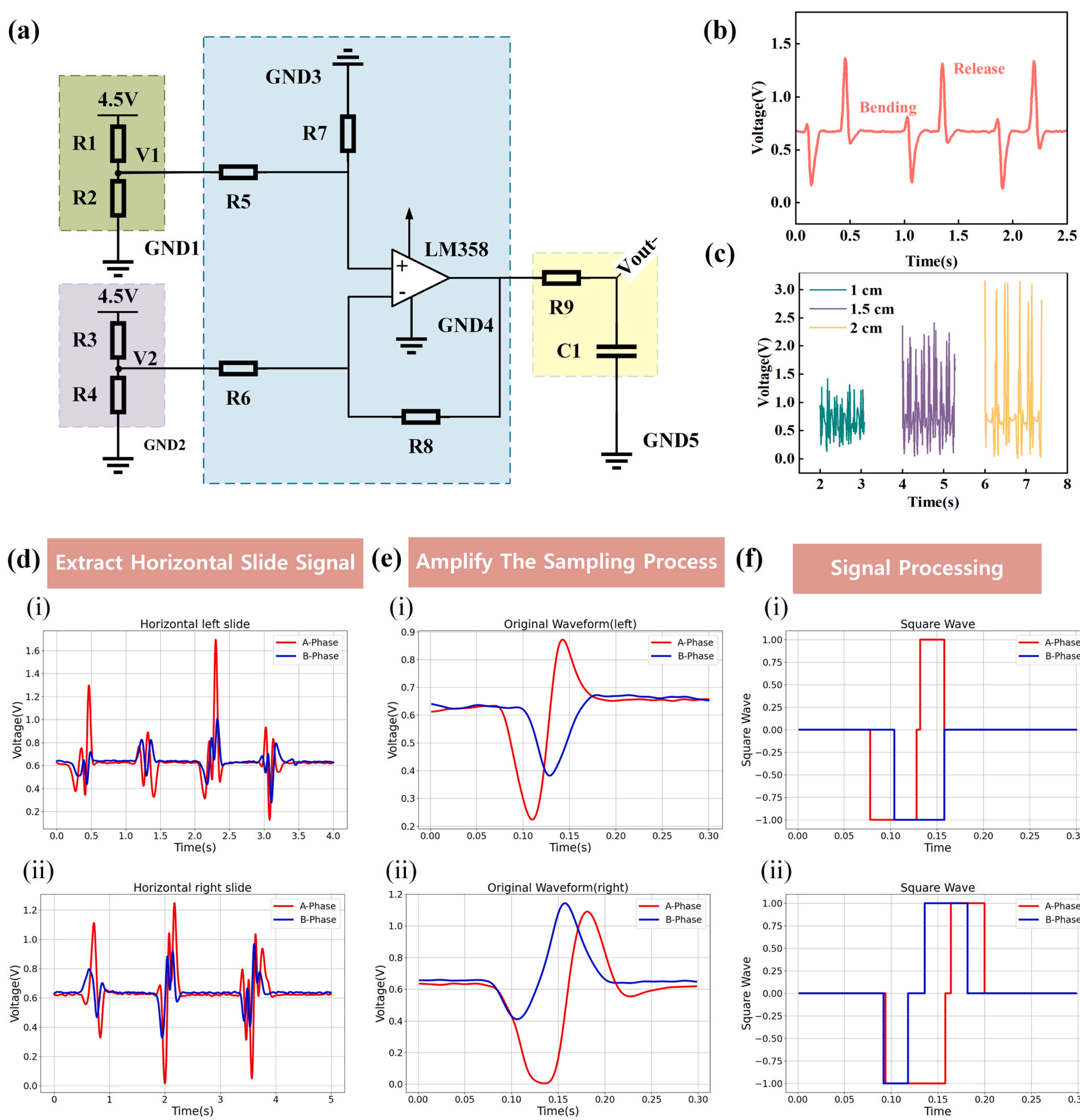

Fig. 3. Signal Processing and Analysis. (a) Schematic of differential signal amplification and filtering based on dual op amps (LM358P). (b) Amplified signal characterization (one complete cycle). (c) Voltage values for different electrode widths. (d) Voltage values for horizontal (i) sliding to the left (ii) sliding to the right. (e) Enlarged view of the slow sliding of the plane (i) to the left (ii) to the right. (f) Setting the threshold for converting (e) into a square wave.

divider resistor is combined with a differential amplifier to establish a continuous input voltage difference higher than zero. This arrangement is designed to increase the amplitude of the signal and then remove unwanted noise by utilizing an RC filter. The calculating formula is demonstrated in Equation S1. A consistent positive signal output may be achieved by considering the virtual short-circuit and virtual open-circuit characteristics.

The act of bending and releasing represents a complete action cycle. As depicted in Fig. 3b, the original AC signal is offset by approximately 0.6 V, resulting in unique waveforms containing both positive and negative cycles, which are suitable for further investigation. The arrangement of electrodes over a surface can generate different levels of electric charge. The stationary end is securely attached to a smooth tabletop to evaluate the sensor's performance. When comparing the sensor output for three different electrode widths (as shown in Fig. 3c), voltage is increased from less than 1.5 V to around 3 V as the contact area becomes more extensive. To achieve accuracy in manufacturing and responsiveness to manual tasks, an electrode width of 1.5 cm is used, except for the outer portions of the thumb. This choice reduces the effects of mutual interference between finger peripherals and guarantees a greater voltage output. Due to the thumb's increased autonomy, greater separation from the other fingers, and restricted range of joint movement, a larger region is selected to address minor discrepancies efficiently.

The signal processing pathway is created based on the principles mentioned above. Data is collected by sliding a single finger horizontally in both directions to evaluate the performance of the two-way signal. Fig. 3d illustrates gathering a two-way signal that displays variations in both amplitude and phase. To provide more elucidation, the sampling frequency is decreased, and the waveforms are scrutinized. The initial waveforms of leftward and rightward sliding are depicted in state(i) and state(ii) of Fig. 3e, respectively. When a sinusoidal signal is processed by a comparator at typical transistor-transistor logic (TTL) levels, it is transformed into a stable square wave signal without any changes to its phase and frequency properties. To replicate the functional implementation of the comparator, a threshold is created in Python to convert the sine wave with DC bias shown in Fig. 3e into three square waves. Once the voltage exceeds a predefined upper threshold, the comparator output is set to 1. Conversely, if the voltage falls below a predefined lower threshold, the output is adjusted to -1. For voltage values that fall within the range between these two thresholds, the comparator output remains at 0. The distinction between the left and right directions can be made by examining the correlation between the signal edges and levels shown in Fig. 3f. Figure S5 presents a detailed portrayal of the dual-channel waveforms associated with an array of directional movements. During the phase of forward motion, it becomes evident that both waveforms undergo same fluctuations, with disparities in their cyclical durations manifesting as varied times of attainment at the conclusion of the motion cycle. During the phase of reverse motion, the A-Phase initiates its change before the corresponding change in the other waveform. Notably, despite this sequential initiation, both channels' waveforms reach a synchronized state at the zero potential position due to their left-aligned structure. This phenomenon is in accordance with the design principles previously elaborated upon in our discourse.

2.4. Experimental characterizations of the PTS

While traditional gesture recognition tends to focus on overall hand movements, examining the individual movement of joints separately from their synergistic effects can provide a more detailed data analysis, revealing additional details of the movements. It is established that the bending behavior of a single finger is primarily executed by the metacarpophalangeal (MCP), proximal interphalangeal (PIP), and distal interphalangeal (DIP) joints. The skeletal and articular structure of the fingers enables the PIP and distal DIP to coordinate with each other during natural flexion. In contrast to the attachment, the DIP is capable of functioning with greater independence. However, the realization of such gestures requires the assistance of the MCP. To reduce the complexity of the distinction, the approach considers PIP and DIP as common motion subjects, focusing on determining the influence of the MCP on this community. The finger's flexion and extension are considered a complete cycle of motion, allowing for an analysis of the impact of frequency and angle on the resulting output. As observed in Fig. 4a and Figure S6, the output of the double-joint flexion process exhibits an increasing number of peaks as the angle is increased. The amplitude of the output remains relatively constant, primarily since a single operating frequency is controlled to achieve an output performance that aligns with the free-standing mode. Fig. 4b depicts the sensor's output voltage as a function of frequency for a fixed entire cycle of bending at 15 degrees. The output voltage exhibits an upward trend followed by a descending trend when the frequency ranges from 0.5 Hz to 2 Hz. The peak output value is achieved at a frequency of 1.5 Hz. Moreover, a higher frequency causes a decrease in the region where friction is effective, resulting in a reduction of friction performance. By combining the advantages of the design above, the two-way signal curve emerges under the synergistic change of frequency and angle (Fig. 4c). A comparison of the graphs under three different conditions reveals that the output amplitude is elevated as the frequency increases. While the bending angle increases, the number of peaks in the signal also increases. This finding is consistent with the observations in Figs. 4a and 4b. A more comprehensive understanding can be gained once the upper signal is considered the primary path and the lower signal is regarded as the phase-assisted directional perception. The discrepancy in the number of peaks observed in the two-path signal can be primarily attributed to its coverage area. Following the same curved route, the two sections will detect varying quantities of primary peaks (Fig. 4d). A linear relationship between the double-joint bending angle and the distance traveled can be observed when fitting the five fingers (Fig. 4e). Except for the thumb, which exhibited an independent distribution, the remaining four fingers demonstrated a comparable linear trend due to their analogous lengths. The variations influenced the discrepancies in the horizontal moving distance distribution of the knuckles' lengths. During the experiment, a thin line with scale markings is affixed at the distal end of the mobile segment. Each measurement ensured that the mobile end aligned with the pipe's leftmost part (near the palm position) initially. The experiments demonstrate that the output of the existing operating principle can support the device in detecting finger flexion movements.

Assess the output variability when the MCP is unable to sustain stable conditions by measuring the horizontal displacement of the five fingers across a range of angles during MCP actuation. The MCP is fixed at 30 degrees due to its typically modest range of motion. As perceived in Fig. 4f, all four fingers, except the ring finger, exhibit satisfactory linearity up to 60 degrees of bending. Moreover, once the bending goes beyond 90 degrees, the displacement length increases instantly, breaking the original linear equilibrium. To argue this point, the outputs under both linear and nonlinear forces are tested for bending degrees of curvature exceeding or equal to 90 degrees. In Fig. 4g, when the MCP joint is maintained in a horizontal position, the uniform flexion of the first two phalangeal joints leads to a distribution of significantly pronounced positive and negative peaks with more consistent amplitudes. Once the MCP is moved in unison, the resulting changes in output are erratic. A transient increase in amplitude is observed, followed by a rapid decrease. Based on the analysis of the reasons, it can be postulated that when the individual finger joints are bent, the bending force is mainly concentrated at a joint of the finger, involving smaller muscle groups, and the distribution of the force is more concentrated, resulting in a relatively stable signal amplitude. Whenever the three joints are flexed, the force distribution becomes less concentrated, resulting in an overall increase in the total force. This leads to a progressive rise in amplitude—the complex intermuscular nervous system (INS) results in complicated linear motions and reduced frequency consistency. If the

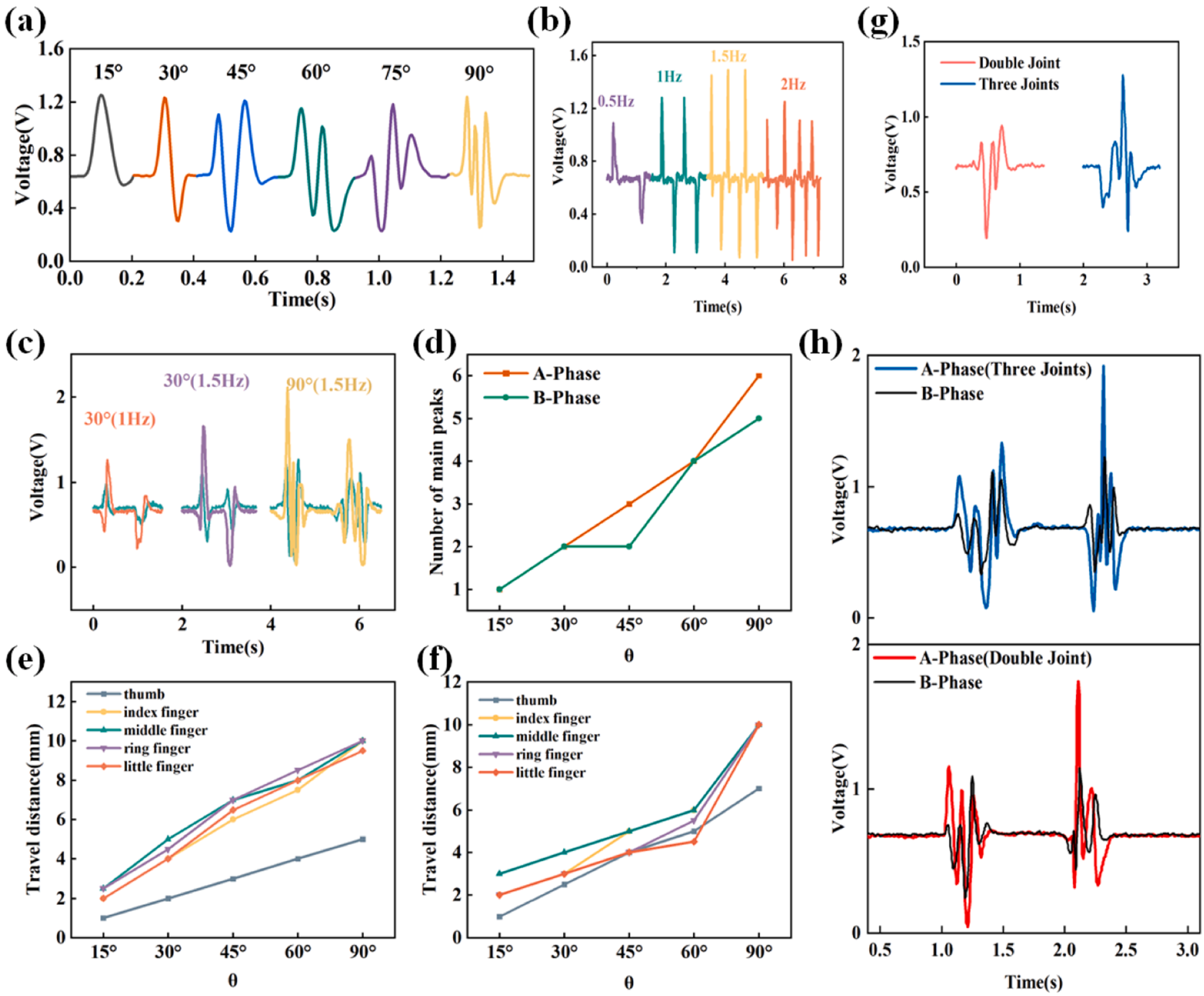

Fig. 4. Characterization of bidirectional sensing systems. (a) The output displays the controlled horizontal sliding of the double-joint at varying angles, all at a consistent frequency (half cycle). (b) The waveform output generated by the bi-directional sensors bending at an angle of 15° is observed at varying frequencies (full cycle). (c) Capture the difference between the two-way signals to distinguish the direction of motion. (d) Establish a relationship between the number of main peaks of the two signals and the bending angle. (e) The five fingers traverse the horizontal distance with angle change during double-joint movement. (f) The horizontal movement distance of the five fingers with angle change under three-joint synergy. (g) The sensor detects differentiated output signals for different joint configurations. (h) Comparison of dual signal outputs in two cases.

flexion angle is too large, the tension in the tendon may surpass the ideal range for transmitting force, leading to inefficient force transmission and a decrease in amplitude. To enable comparison, a complete cycle of movement is executed, consisting of an initial phase of joint bending and a subsequent phase of releasing the movement after bending (Fig. 4h). On the one hand, variations in both linear and nonlinear movement patterns are noticeable during the flexion phase. On the other hand, the process of releasing something experiences a temporary and abrupt alteration caused by the finger being pulled back, caused by the sliding of the sensor. By integrating the phase information of the lower signal, a more comprehensive understanding of the motion may be obtained.

2.5. Deep learning based single finger state analysis

Figure S7 shows an image of the overall modular layout. The two signals from a single finger are interfaced with the analog input terminals of a microcontroller unit (MCU), specifically an Arduino Nano 33 BLE, after which they are subjected to amplification. To ensure compatibility with the MCU's integrated analog-to-digital converter (ADC), a DC bias is incorporated into the signals, thereby aligning them with the ADC's read range. Furthermore, the MCU's integrated step-down module is utilized to adapt the chip's power supply to meet the 3.3 V requirement, while the built-in low-power Bluetooth module facilitates long-distance, low-power wireless data transmission, enhancing the system's overall efficiency and functionality. The microprocessor is equipped with eight analog input interfaces. To accommodate the simultaneous input from all five fingers, requiring ten analog input channels, an external multiplexer (MCP3008) widens the system's capabilities. Additionally, the system, utilizing PyCharm, integrates the Bleak and PyQtGraph libraries to wirelessly receive data from the MCU and to provide real-time graphing of multi-channel signals on the graphical interface, as shown in Figure S8.

Characterizing the flexion and extension states of a single finger joint involves sampling data across a range of angles and frequencies rather than refining the bending angle. This strategy aims to develop a more robust model. Fig. 5a illustrates the ability of the three-layer CNN model

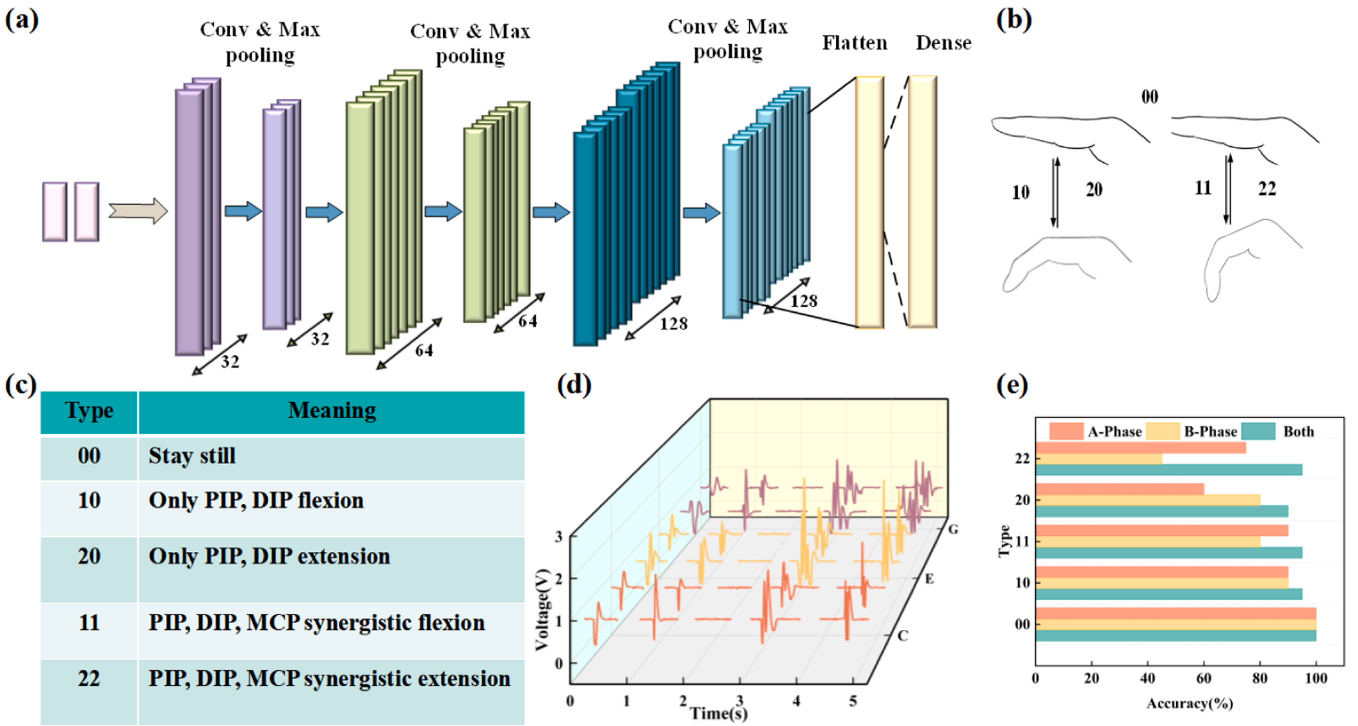

Fig. 5. Single-finger motion state recognition and analysis. (a) Neural network classification model based on two-channel CNN. (b) Classification results: digits are used to refer to different joint states. (c) Representation of the exact meaning of the classification and recognition results. (d)Acquired dual-channel signal waterfall diagram (x-axis: different motion states, y-axis: multiple sampling processes in the same state, z-axis: the magnitude of the voltage output of the signal). (e) Comparison of classification accuracy under dual-channel and single-channel.

to process dual-channel voltage data simultaneously. The convolutional operations across multiple channels capture distinct information from each channel, resulting in a more comprehensive and nuanced feature representation. Dimensionality reduction techniques, including Principal Component Analysis (PCA) and t-distributed Stochastic Neighbor Embedding (t-SNE), are utilized to project high-dimensional data into a lower-dimensional space, while classification labels are converted to a one-hot encoding format. The model training incorporated the ReduceLROnPlateau callback function, which reduces the learning rate by a specified factor if the monitored metric (val_loss) shows no improvement over a set number of epochs. Learning rate scheduling and model checkpoint callback functions are employed to adjust the training process dynamically, optimizing the parametric model. The predicted results are indicated by three numbers representing joint movement: 0 for maintaining the original position, 1 for forward movement, and 2 for backward extension (Fig. 5b), as detailed meaning in Fig. 5c. Accurate prediction of joint motion states enables precise gesture estimation and repositioning.

Executing a series of repeated finger flexion and extension movements, research amassed comprehensive data on flexion across a variety of states and frequencies (Fig. 5d). Each channel is sampled with 200 data points and repeated 100 times at different intervals. Analysis of the waveform information reveals distinct patterns for flexion and extension in the double-joint configuration, including various flexion situations below 90 degrees, to enhance the model's generalization and mitigate overfitting. Compared to the double-joint, the three-joint synergistic scenario exhibited more pronounced waveform changes sampled at larger bending amplitudes. The upward-only, downward-only, and dual-channel signals are compared to assess improvements in dual-channel prediction performance. In examining the confusion matrix depicted in Figure S9, a notable enhancement in the prediction accuracy for each joint motion is discernible upon the utilization of dual-channel signals, as evidenced in Fig. 5e.

2.6. *Real-time gesture monitoring aids robot imitation learning*

For single-finger signals, distinguishing different motion states can be achieved through peak count or signal amplitude due to their limited information dimension. Nevertheless, discerning data discrepancies through visual inspection becomes challenging for complex gestures that entail interactions across multiple joints. Additionally, finger tremors induced by fatigue can introduce variability in the signal patterns. This study employs machine learning to capture subtle differences for accurate classification, optimizing the previously designed single-finger model. The experimental system, shown in Fig. 6a, integrates sensors with Unity for real-time gesture imitation and interaction. Machine learning-based object recognition translates voltage features into digital commands, simplifying the mapping of object information into virtual space. To improve prediction accuracy, the CNN model is refined with ten channels of data, with each channel sampled at 150 points (Figure S10). The channels are grouped into five pairs, with shared convolutional layers used for feature extraction to better capture local correlations between sensor channels from the same finger. Figure S11 exhibits the outcomes of the visualization process, wherein gestures from various categories are discernible and well-separated.

The model's performance is evaluated by comparing it with several alternatives: multi-channel Convolutional Neural Network (CNN), multi-channel Convolutional Neural Network-Long Short Term Memory (CNN-LSTM), and our shared convolutional layers-Convolutional Neural Network(SCL-CNN) model. The confusion matrices for predictions are presented in Fig. 6b and Figure S12. Table 1 details the classification accuracy for each model. Although the CNN-LSTM architecture captures temporal dependencies in conjunction with spatial features, its accuracy decreased, likely owing to weak temporal correlations within our data and increased model complexity, which led to overfitting. Notably, the confusion matrices, particularly for the multi-channel CNN model, indicate that the primary cause of accuracy reduction stems from misclassifications between gestures 0 (fist) and 2 (five-finger spread), which

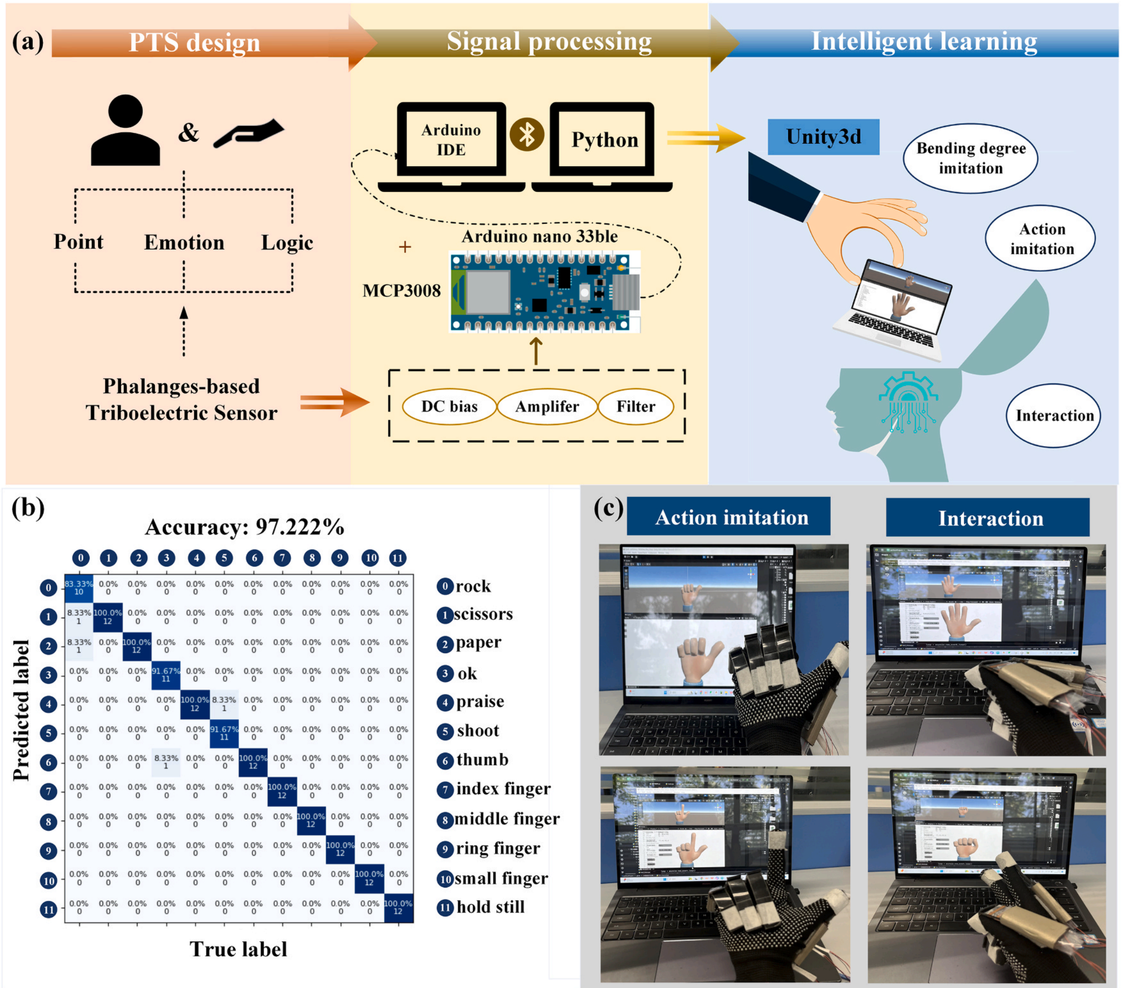

Fig. 6. Experimental system for real-time acquisition. (a) Overall experimental flowchart. (b)Accuracy confusion matrix for gesture imitation. (c) The learning interface is constructed through the Unity platform. This includes action imitation and interaction.

Table 1
Prediction accuracy of different models.

Model	Accuracy(%)
CNN	94.444
CNN-LSTM	87.5
SCL-CNN	97.222

exhibit similar complexity and dynamics. In contrast, the enhanced SCL-CNN model achieves over 97 % accuracy, demonstrating that shared feature spaces can substantially improve prediction performance. This advancement supports greater control precision in virtual interactions, enhancing user experience. The Unity3D-based intelligent interface, as showcased in the supplementary Video S1, replicates operator gestures with a virtual hand, which can be trained to transition from mimicking the bending of a single finger to imitating complex gestural movements, even in the absence of a camera. Through engagement with the game, the robot can comprehend the underlying mechanics through the outcomes of human actions, thereby gradually acquiring the capacity to master the rules. Fig. 6c and S13 illustrate the virtual hand's capability to imitate human gestures, conduct simple interactions, and refine the accuracy of complex movements to accommodate varied interactive needs.

Supplementary material related to this article can be found online at doi:10.1016/j.nanoen.2024.110491.

Supplementary material related to this article can be found online at doi:10.1016/j.nanoen.2024.110491.

2.6.1. *Smart glove integrated with large-scale model for real-time interaction*

Fig. 7a depicts the core structure of an intelligent system composed of three main components: perception, intelligent decision-making, and action implementation. The intelligent system is designed to dynamically adapt to environmental changes by processing multidimensional sensory inputs—including auditory, visual, and tactile data—through its perception module. In this framework, the human operator utilizes data gloves to enhance the application of deep learning techniques, thereby enabling continuous improvement in the system's intelligence. The decision-making layer, represented by the brain, manages critical functions such as data storage and response generation. By integrating a large language model as an interface, the robot progressively acquires the capability to execute actions through natural language interactions.

Fig. 7b showcases the User Interface (UI). The robot's learning capacity is augmented by integrating linguistic and gestural inputs, which fosters its development into a fully autonomous intelligent entity. Supplementary Video S2 presents a comprehensive overview of the demonstration process. The correct execution of a greeting gesture forms the foundation for identity verification, thereby ensuring the confidentiality of information (Fig. 7b(i)). Additionally, in Fig. 7b(ii), the robot, activated by a designated wake word and equipped with dual-layer encryption, can respond verbally, thus minimizing the risk of misuse. The integration of gestural commands enables the robot to perform basic

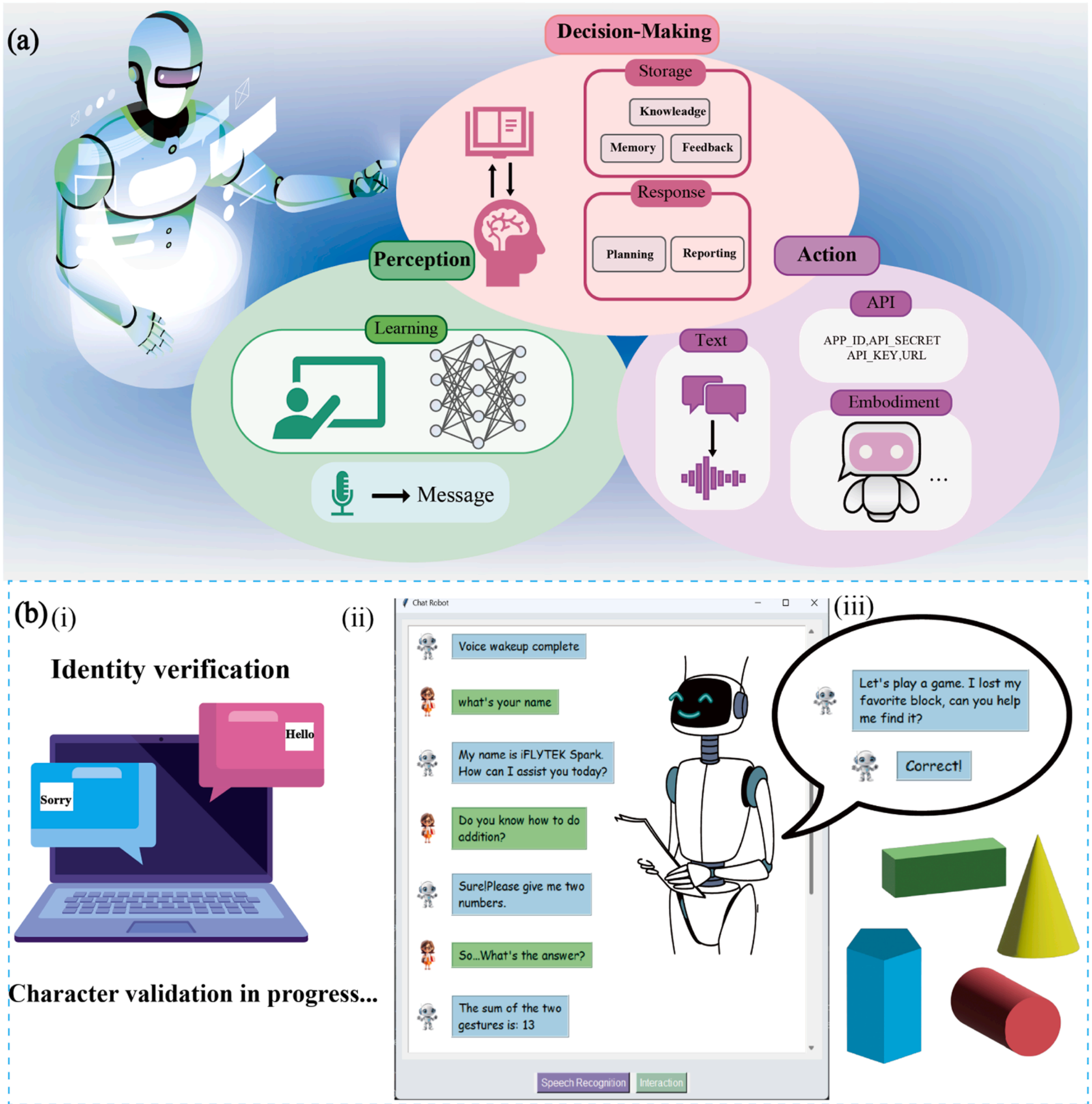

Fig. 7. Gesture-Based Growth Large Language Model (LLM) Robot System. (The Large Language Model is derived from the iFLYTEK Model). (a) The overall architecture of the intelligent system. (b) A stand-alone Teaching Interface (Ti-EAI) enables the robot to execute various tasks: (i) Character authentication for secure and confidential access control. (ii) Integration of voice and gesture interaction for dialog and logical reasoning with the robot. (iii) Interaction with the robot through smart gloves allows the user to distinguish between block shapes and engage in interactive gaming.

mathematical operations and engage in more meaningful interactions with humans beyond traditional computational environments, enriching the gaming experience (Fig. 7b(iii)).

3. Conclusion

In summary, this research introduces a novel wearable teaching interface designed to empower robots with the capability to autonomously acquire knowledge. Our design incorporates a self-powered triboelectric nanogenerator (TENG) sensing mechanism and introduces an advanced electrode configuration that strategically employs phase differential principles, featuring electrodes of diverse widths for optimized performance. This innovative combination allows for the creation of smart gloves with high precision to detect a wide array of intricate hand gestures. Furthermore, this work incorporates the use of shared convolutional layers within a Convolutional Neural Network (CNN) model, resulting in remarkable precision in distinguishing both individual finger joint states and the overall execution of hand gestures, with a success rate surpassing 95 %. Additionally, an online intelligent education platform has been developed, which harnesses large-scale models and Unity3D technology to seamlessly integrate sensors with cutting-edge machine learning and AI technologies. By enhancing the mimetic learning abilities of the robots, this platform facilitates the achievement of dialogue, recognition, and teaching tasks within the robot's system, ultimately offering an immersive and engaging educational experience. Overall, this research contributes significantly to the advancement of Embodied AI and wearable technology, establishing the foundation for future innovative educational applications.

4. Experimental section

4.1. The fabrication process of the Phalanges-based Triboelectric Sensor (PTS)

As depicted in Figure S14, the fabrication process involves constructing two main components: a fixed end and a movable end. A 1 mm EVA foam layer is laminated onto a PVC film to serve as the supporting framework of the device. The length of each segment is predetermined by measuring the distances between the finger joints, and the connecting components are cut to these lengths using laser cutting. The width of each component is set to 1.5 cm, slightly longer than the finger's width (2 cm for the thumb). Once the cutting process is complete, the components are assembled. For the fixed end of the tubular structure, interdigitated electrodes made from 3 mm wide copper foil tape are arranged with a 1 mm gap on the inner surfaces, and a 0.1 mm FEP film is applied as the critical triboelectric material. For the movable end, grid copper electrodes of different widths (3 mm on the top and 5 mm on the bottom) are applied to the upper and lower surfaces. The tubular structure of the fixed end has openings at both ends, allowing the linkage structure to slide freely within the tube as the finger joints move.

CRediT authorship contribution statement

Dezhi Yin: Visualization. **Yifeng Su:** Visualization. **Xinmao Zhao:** Writing – original draft, Visualization, Validation, Software, Resources, Methodology, Formal analysis, Data curation. **Tong Hu:** Writing – original draft, Visualization, Validation, Software, Formal analysis, Data curation. **Zhonglin Wang:** Supervision, Funding acquisition. **Chengkuo Lee:** Supervision, Funding acquisition. **Long Liu:** Writing – review & editing, Visualization, Validation, Supervision, Software, Resources, Project administration, Methodology, Investigation, Funding acquisition, Formal analysis, Data curation, Conceptualization.

Declaration of Competing Interest

The authors declare that they have no known competing financial interests or personal relationships that could have appeared to influence the work reported in this paper.

Acknowledgments

This work is supported by "Guangdong Basic and Applied Basic Research Foundation" (2023A1515110229).

Supporting information

Supplementary data associated with this article can be found in the online version.

Appendix A. Supporting information

Supplementary data associated with this article can be found in the online version at doi:10.1016/j.nanoen.2024.110491.

Data Availability

Data will be made available on request.

References

[1] A. Gupta, S. Savarese, S. Ganguli, L. Fei-Fei, Embodied intelligence via learning and evolution, Nat. Commun. 12 (2021) 5721, https://doi.org/10.1038/s41467-021-25874-z.
[2] L. Foglia, R.A. Wilson, Embodied cognition, WIREs Cogn. Sci. 4 (2013) 319–325, https://doi.org/10.1002/wcs.1226.
[3] Y. Jiang, L. Fan, H. Wang, Z. Luo, W. Zhang, J. Wang, X. Sun, N. Li, J. Tian, Highly resilient aerogel/sponge nested structures assisted multimodal tactile sensory system for robotic embodied perception, Nano Energy 131 (2024) 110279, https://doi.org/10.1016/j.nanoen.2024.110279.
[4] J. Duan, S. Yu, T. Li, H. Zhu, C. Tan, A survey of embodied AI: from simulators to research tasks, IEEE Trans. Emerg. Top. Comput. Intell. 6 (2021) 230–244, https://doi.org/10.1109/TETCI.2022.3141105.
[5] O.M. Andrychowicz, B. Baker, M. Chociej, R. Józefowicz, B. McGrew, J. Pachocki, A. Petron, M. Plappert, G. Powell, A. Ray, J. Schneider, S. Sidor, J. Tobin, P. Welinder, L. Weng, W. Zaremba, Learning dexterous in-hand manipulation, Int. J. Robot. Res. 39 (2020) 3–20, https://doi.org/10.1177/0278364919887447.
[6] S. Han, B. Liu, R. Cabezas, C.D. Twigg, P. Zhang, J. Petkau, T.-H. Yu, C.-J. Tai, M. Akbay, Z. Wang, A. Nitzan, G. Dong, Y. Ye, L. Tao, C. Wan, R. Wang, MEgATrack: monochrome egocentric articulated hand-tracking for virtual reality, Article 87. ACM Trans. Graph. 39 (2020) https://doi.org/10.1145/3386569.3392452.
[7] K.M. Park, J. Kim, J. Park, F.C. Park, Learning-based real-time detection of robot collisions without joint torque sensors, IEEE Robot. Autom. Lett. 6 (2021) 103–110, https://doi.org/10.1109/LRA.2020.3033269.
[8] S.P. Arunachalam, S. Silwal, B. Evans, L. Pinto, Dexterous imitation made easy: a learning-based framework for efficient dexterous manipulation, 2023 IEEE Int. Conf. Robot. Autom. (ICRA) (2023) 5954–5961, https://doi.org/10.1109/ICRA48891.2023.10160275.
[9] B. Kim, J.Y. Song, D.Y. Kim, M.W. Cho, J.G. Park, D. Choi, C. Lee, S.M. Park, Environmentally robust triboelectric tire monitoring system for self-powered driving information recognition via hybrid deep learning in time-frequency representation, Small 20 (2024) 2400484, https://doi.org/10.1002/smll.202400484.
[10] K.L. Valenzuela, S.I. Roxas, Y.-H. Wong, Embodying Intelligence: Humanoid Robot Advancements and Future Prospects, Springer Nature Switzerland, 2024, pp. 295–303, https://doi.org/10.1007/978-3-031-60615-1_20.
[11] R. Pfeifer, F. Iida, Embodied Artificial Intelligence: Trends and Challenges, in: Springer Berlin Heidelberg, 2004, pp. 1–26, https://doi.org/10.1007/978-3-540-27833-7_1.
[12] P. Li, H. Jeong, The social brain of language: grounding second language learning in social interaction, npj Sci. Learn. 5 (2020) 8, https://doi.org/10.1038/s41539-020-0068-7.
[13] J. Pearson, The human imagination: the cognitive neuroscience of visual mental imagery, Nat. Rev. Neurosci. 20 (2019) 624–634, https://doi.org/10.1038/s41583-019-0202-9.
[14] E. Zima, G. Brône, Cognitive Linguistics and interactional discourse: time to enter into dialogue, Lang. Cogn. 7 (2015) 485–498, https://doi.org/10.1017/langcog.2015.19.
[15] R. Coll, B. France, I. Taylor, The role of models and analogies in science education: implications from research, Int. J. Sci. Educ. 27 (2005) 183–198, https://doi.org/10.1080/0950069042000276712.
[16] Y. Dai, Z. Lin, A. Liu, W. Wang, An embodied, analogical and disruptive approach of AI pedagogy in upper elementary education: an experimental study, Br. J. Educ. Technol. 55 (2024) 417–434, https://doi.org/10.1111/bjet.13371.
[17] X. Li, R. Wen, Z. Shen, Z. Wang, K.D.K. Luk, Y. Hu, A wearable detector for simultaneous finger joint motion measurement, IEEE Trans. Biomed. Circuits Syst. 12 (2018) 644–654, https://doi.org/10.1109/TBCAS.2018.2810182.
[18] G. Yuan, X. Liu, Q. Yan, S. Qiao, Z. Wang, L. Yuan, Hand gesture recognition using deep feature fusion network based on wearable sensors, IEEE Sens. J. 21 (2021) 539–547, https://doi.org/10.1109/JSEN.2020.3014276.
[19] T. He, Z. Sun, Q. Shi, M. Zhu, D.V. Anaya, M. Xu, T. Chen, M.R. Yuce, A.V.-Y. Thean, C. Lee, Self-powered glove-based intuitive interface for diversified control applications in real/cyber space, Nano Energy 58 (2019) 641–651, https://doi.org/10.1016/j.nanoen.2019.01.091.
[20] M.L. Zhu, T.Y.Y. He, C.K. Lee, Technologies toward next generation human machine interfaces: From machine learning enhanced tactile sensing to neuromorphic sensory systems, Appl. Phys. Rev. 7 (2020) 031305, https://doi.org/10.1063/5.0016485.
[21] B.S. Lin, P.C. Hsiao, S.Y. Yang, C.S. Su, I.J. Lee, Data glove system embedded with inertial measurement units for hand function evaluation in stroke patients, IEEE Trans. Neural Syst. Rehabil. Eng. 25 (2017) 2204–2213, https://doi.org/10.1109/TNSRE.2017.2720727.
[22] J. Connolly, J. Condell, B. O'Flynn, J.T. Sanchez, P. Gardiner, IMU sensor-based electronic goniometric glove for clinical finger movement analysis, IEEE Sens. J. 18 (2018) 1273–1281, https://doi.org/10.1109/JSEN.2017.2776262.
[23] J. Kim, M. Lee, H.J. Shim, R. Ghaffari, H.R. Cho, D. Son, Y.H. Jung, M. Soh, C. Choi, S. Jung, K. Chu, D. Jeon, S.-T. Lee, J.H. Kim, S.H. Choi, T. Hyeon, D.-H. Kim, Stretchable silicon nanoribbon electronics for skin prosthesis, Nat. Commun. 5 (2014) 5747, https://doi.org/10.1038/ncomms6747.
[24] C. Wu, A.C. Wang, W. Ding, H. Guo, Z.L. Wang, Triboelectric nanogenerator: a foundation of the energy for the new era, Adv. Energy Mater. 9 (2018) 1802906, https://doi.org/10.1002/aenm.201802906.
[25] X. Cui, C. Yu, Z. Wang, D. Wan, H. Zhang, Triboelectric nanogenerators for harvesting diverse water kinetic energy, Micro (Basel) 13 (2022) 1219, https://doi.org/10.3390/mi13081219.
[26] J. Yin, V. Kashyap, S. Wang, X. Xiao, T. Tat, J. Chen, Self-powered eye-computer interaction via a triboelectric nanogenerator, Device 2 (2024) 100252, https://doi.org/10.1016/j.device.2023.100252.
[27] N. Tiwari, M. Lazzari, Thermosensitive wearable sensing technologies with intelligent robotics, Device 2 (2024) 100362, https://doi.org/10.1016/j.device.2024.100362.
[28] K. Tao, J. Yu, J. Zhang, A. Bao, H. Hu, T. Ye, Q. Ding, Y. Wang, H. Lin, J. Wu, H. Chang, H. Zhang, W. Yuan, Deep-learning enabled active biomimetic multifunctional hydrogel electronic skin, ACS Nano 17 (2023) 16160–16173, https://doi.org/10.1021/acsnano.3c05253.
[29] T. Wang, T. Jin, W. Lin, Y. Lin, H. Liu, T. Yue, Y. Tian, L. Li, Q. Zhang, C. Lee, Multimodal sensors enabled autonomous soft robotic system with self-adaptive manipulation, ACS Nano 18 (2024) 9980–9996, https://doi.org/10.1021/acsnano.3c11281.
[30] S. Liu, S. An, X. Zhou, J. Wang, X. Pu, A self-powered, process-oriented wireless sensor with high discharge signal density, Device 2 (2024) 100437, https://doi.org/10.1016/j.device.2024.100437.
[31] J. Xu, X. Pan, B. Xu, H. Yue, Y. Lu, K. Ying, Z. Wang, F. Yang, Buckling-inspired triboelectric sensor for multifunctional sensing of soft robotics and wearable

devices, Nano Energy 130 (2024) 110141, https://doi.org/10.1016/j.nanoen.2024.110141.

[32] X. Dan, X. Cao, Y. Wang, J. Yang, Z.L. Wang, Q. Sun, A stereoscopically structured triboelectric nanogenerator for bending sensors and hierarchical interactive systems, ACS Appl. Nano Mater. 6 (2023) 3590–3598, https://doi.org/10.1021/acsanm.2c05360.

[33] L. Wang, Z. Fei, Z. Wu, Y. Ye, Y. Qi, J. Wang, L. Zhao, C. Zhang, Y. Zhang, G. Qin, Z. Jiang, R. Maeda, Wearable bending wireless sensing with autonomous wake-up by piezoelectric and triboelectric hybrid nanogenerator, Nano Energy (2023) 108504, https://doi.org/10.1016/j.nanoen.2023.108504.

[34] P. Fang, M.-I. Zhu, Z.-B. Zeng, W.-X. Lu, F.-X. Wang, L. Zhang, T. Chen, L.-N. Sun, A multi-module sensing and Bi-directional HMI integrating interaction, recognition, and feedback for intelligent robots, Adv. Funct. Mater. 34 (2024) 2310254, https://doi.org/10.1002/adfm.202310254.

[35] Y. Xiong, Z. Huo, J. Zhang, Y. Liu, D. Yue, N. Xu, R. Gu, L. Wei, L. Luo, M. Chen, C. Liu, Z.L. Wang, Q. Sun, Triboelectric in-sensor deep learning for self-powered gesture recognition toward multifunctional rescue tasks, Nano Energy 124 (2024) 109465, https://doi.org/10.1016/j.nanoen.2024.109465.

[36] S. Zhang, S.M.S. Rana, T. Bhatta, G.B. Pradhan, S. Sharma, H. Song, S. Jeong, J. Y. Park, 3D printed smart glove with pyramidal MXene/Ecoflex composite-based toroidal triboelectric nanogenerators for wearable human-machine interaction applications, Nano Energy 106 (2023) 108110, https://doi.org/10.1016/j.nanoen.2022.108110.

[37] L. Wen, M. Nie, P. Chen, Y.-N. Zhao, J. Shen, C. Wang, Y. Xiong, K. Yin, L. Sun, Wearable multimode sensor with a seamless integrated structure for recognition of different joint motion states with the assistance of a deep learning algorithm, Microsyst. Nanoeng. 8 (2022) 24, https://doi.org/10.1038/s41378-022-00358-2.

[38] M. Zhu, Z. Sun, T. Chen, C. Lee, Low cost exoskeleton manipulator using bidirectional triboelectric sensors enhanced multiple degree of freedom sensory system, Nat. Commun. 12 (2021) 2692, https://doi.org/10.1038/s41467-021-23020-3.

[39] M. Santello, G. Baud-Bovy, H. Jörntell, Neural bases of hand synergies, Front. Comput. Neurosci. 7 (2013), https://doi.org/10.3389/fncom.2013.00023.

[40] R. Takahashi, N. Miyata, Y. Maeda, K. Fujita, Grasp synthesis for digital hands with limited range of motion in their thumb joints, IEEE Int. Conf. Syst. Man Cybern. (SMC) 2019 (2019) 181–186, https://doi.org/10.1109/SMC.2019.8914453.

[41] M. Zhu, Z. Sun, C. Lee, Soft modular glove with multimodal sensing and augmented haptic feedback enabled by materials' multifunctionalities, ACS Nano 16 (2022) 14097, https://doi.org/10.1021/acsnano.2c04043.

[42] X. Xie, Q. Wang, C. Zhao, Q. Sun, H. Gu, J. Li, X. Tu, B. Nie, X. Sun, Y. Liu, E.G. Lim, Z. Wen, Z.L. Wang, Neuromorphic computing-assisted triboelectric capacitive-coupled tactile sensor array for wireless mixed reality interaction, ACS Nano 18 (2024) 17041–17052, https://doi.org/10.1021/acsnano.4c03554.

[43] P. Vijayalakshmi, D.D. Karthika, Ensemble classification based hybrid dual-channel convolution neural network (dccnn) with enhanced manta ray foraging optimization (emrfo) algorithm for cyber security malware threats detection, Salud, Cienc. Y. Tecnol. ía - Ser. De. Conf. (2024), https://doi.org/10.56294/sctconf2024760.

[44] T. Sun, C. Yao, Z. Liu, S. Huang, X. Huang, S. Zheng, J. Liu, P. Shi, T. Zhang, H. Chen, H.-J. Chen, X. Xie, Machine learning-coupled vertical graphene triboelectric pressure sensors array as artificial tactile receptor for finger action recognition, Nano Energy 123 (2024) 109395, https://doi.org/10.1016/j.nanoen.2024.109395.

[45] A. Babu, D. Mandal, Roadmap to human–machine interaction through triboelectric nanogenerator and machine learning convergence, ACS Appl. Energy Mater. 7 (2024) 822–833, https://doi.org/10.1021/acsaem.3c02642.

[46] Y. Li, M. Qin, Q. Lin, J. Liu, S. Wu, Z. Yao, Y. Li, T. Sun, H. Kan, Artificial intelligence motivated flexible single-electrode mode multilayer triboelectric sensor for smart mobility systems, Nano Energy 125 (2024) 109515, https://doi.org/10.1016/j.nanoen.2024.109515.

Long Liu received his Ph.D. degree from the Beijing Institute of Nanoenergy and Nanosystems, Chinese Academy of Sciences in 2018. From 2018–2022, he worked as a Research Fellow in the Department of Electrical and Computer Engineering at the National University of Singapore. Since July 2022, he has been working as a professor and, since July 2023, he has led a research team in the School of Electronics and Information at Northwestern Polytechnical University. His current research interests are focused on fundamental and applied research in nanogenerators, energy harvesters, self-powered sensors, wearable electronics, human-machine interaction, advanced artificial intelligence, and IoT applications.

Tong Hu received her B.Eng. degree in Electrical Engineering and Automation from Changsha University of Science and Technology in 2023. Currently, she is pursuing her M.S. degree in New-Generation Electronic Information Technology at Northwestern Polytechnical University, China. Her research interests are mainly focused on wearable electronics and self-powered sensors.

Xinmao Zhao received his B.Eng. degree in Optoelectronic Information Science and Engineering from North University of China in 2022. Currently, he is pursuing his M.S. degree in Communication Engineering at Northwestern Polytechnical University, China. His research interests are mainly focused on wireless communication and self-powered sensors.

Yifeng Su received his B.Eng. degree in Electronic Information Engineering from Jinan University in 2024. Currently, he is pursuing his M.S. degree in New-Generation Electronic Information Technology at Northwestern Polytechnical University, China. His research interests are mainly focused on self-powered sensors.

Dezhi Yin received his B.Eng. degree in Electronic Information Engineering from Qingdao University in 2024. Currently, he is pursuing his M.S. degree in New-Generation Electronic Information Technology at Northwestern Polytechnical University, China. His research interests are mainly focused on self-powered sensors.

Chengkuo Lee received his Ph.D. degree in Precision Engineering from The University of Tokyo in 1996. Currently, he is the director of Center for Intelligent Sensors and MEMS at National University of Singapore, Singapore. In 2001, he cofounded Asia Pacific Microsystems, Inc., where he was the Vice President. From 2006–2009, he was a Senior Member of the Technical Staff at the Institute of Microelectronics, A-STAR, Singapore. He has contributed to more than 500 peer-reviewed international journal articles. His ORCID is 0000–0002–8886–3649.

Prof. Zhong Lin Wang received his Ph. D from Arizona State University in physics. He now is the Hightower Chair in Materials Science and Engineering, Regents' Professor, Engineering Distinguished Professor and Director, Center for Nanostructure Characterization, at Georgia Tech. Dr. Wang has made original and innovative contributions to the synthesis, discovery, characterization and understanding of fundamental physical properties of oxide nanobelts and nanowires, as well as applications of nanowires in energy sciences, electronics, optoelectronics and biological science. He pioneered the field of piezotronics and piezo-phototronics by introducing piezoelectric potential gated charge transport process in fabricating new electronic and optoelectronic devices.